NANO LETTERS

2008
Vol. 8, No. 5
1501-1505

ZnO Nanostructures as Efficient Antireflection Layers in Solar Cells

Yun-Ju Lee,* Douglas S. Ruby, David W. Peters, Bonnie B. McKenzie, and Julia W. P. Hsu

Sandia National Laboratories, Albuquerque, New Mexico 87185

Received March 4, 2008; Revised Manuscript Received March 26, 2008

ABSTRACT

An efficient antireflection coating (ARC) can enhance solar cell performance through increased light coupling. Here, we investigate solution-grown ZnO nanostructures as ARCs for Si solar cells and compare them to conventional single layer ARCs. We find that nanoscale morphology, controlled through synthetic chemistry, has a great effect on the macroscopic ARC performance. Compared with a silicon nitride (SiN) single layer ARC, ZnO nanorod arrays display a broadband reflection suppression from 400 to 1200 nm. For a tapered nanorod array with average tip diameter of 10 nm, we achieve a weighted global reflectance of 6.6%, which is superior to an optimized SiN single layer ARC. Calculations using rigorous coupled wave analysis suggest that the tapered nanorod arrays behave like modified single layer ARCs, where the tapering leads to impedance matching between Si and air through a gradual reduction of the effective refractive index away from the surface, resulting in low reflection particularly at longer wavelengths and eliminating interference fringes through roughening of the air−ZnO interface. According to the calculations, we may further improve ARC performance by tailoring the thickness of the bottom fused ZnO layer and through better control of tip tapering.

Antireflection coatings (ARCs) play a major role in enhancing the efficiency of photovoltaic (PV) devices by increasing light coupling into the active region of the devices. On lithographically patterned Si PV devices, various groups have fabricated surface textured ARCs by anisotropic etching,[1] etching through patterned masks,[2–5] or via other techniques that generate porosity and/or roughness.[6–8] The textured surface traps light, leading to a broadband suppression in reflection. For thin film PV devices (e.g., amorphous Si, CdTe, $CdInGaSe_2$), ARCs generally consist of one or more dielectric layers, either in the form of a quarter wave thickness film that exhibits a wavelength sensitive reduction in reflection due to interference[9–15] or as a nanoporous film that takes advantage of light trapping for a more broadband response.[16,17] Recently, Xi et al. utilized oblique-angle deposition at different angles to create five layers of TiO_2 and SiO_2 nanorods with an optimized overall refractive index gradient, and achieved an extremely low reflectance.[18] In their case, discontinuous refraction index changes between layers with different volume fractions of dielectrics created the desired refractive index profile. In this communication, we report the effects of highly textured ZnO nanorod arrays (NRAs), synthesized via low temperature solution growth, on ARC performance. By changing the growth conditions, we modify the shape of the ZnO nanorod tips, leading to continuously varying refractive index profiles in a single layer. Subtle changes in the nanorod tip shape result in significantly improved antireflection properties, in good agreement with predictions from rigorous coupled wave analysis (RCWA). Because our approach is substrate independent, these textured ZnO ARCs may be applicable to a wide variety of PV devices and other antireflection applications.

ZnO is attractive as a dielectric ARC material because of its good transparency, appropriate refractive index ($n = 2$), and ability to form textured coating via anisotropic growth. For example, textured ZnO films deposited on Si via metal organic chemical vapor deposition (MOCVD) demonstrated superior ARC performance compared with a TiO_2 single layer ARC (SLARC).[12] We synthesized ZnO NRA ARCs using a two-step seeding and growth method on *n*-type Si(100) (Allied Bendix).[19,20] The seeding process was carried out at room temperature at 35% relative humidity, the optimal condition for producing ordered NRAs.[20] Seeded substrates were placed in aqueous solutions containing zinc nitrate (Fisher) and hexamethylene tetraamine (HMT, Fisher) at 92.5 or 60 °C. Several concentrations of 1,3-diaminopropane (DAP, Acros) were also added to control the tapering of nanorods; see Supporting Information for the full list of ZnO NRAs and their synthesis conditions.[21,22] An example of a ZnO NRA in cross section imaged with a scanning electron microscope (SEM) is shown in Figure 1a. For comparison, a 0.55 μm thick porous ZnO film was also deposited on Si via multiple steps of spin coating a sol of 2 M zinc acetate (Aldrich) and 2 M ethanolamine (Aldrich) in 2-methoxyethanol (Aldrich) at 2000 rpm followed by heating on a hot plate at 300 °C for 5 min.[23]

* Corresponding author. E-mail: ylee@sandia.gov.

10.1021/nl080659j CCC: $40.75
Published on Web 04/17/2008

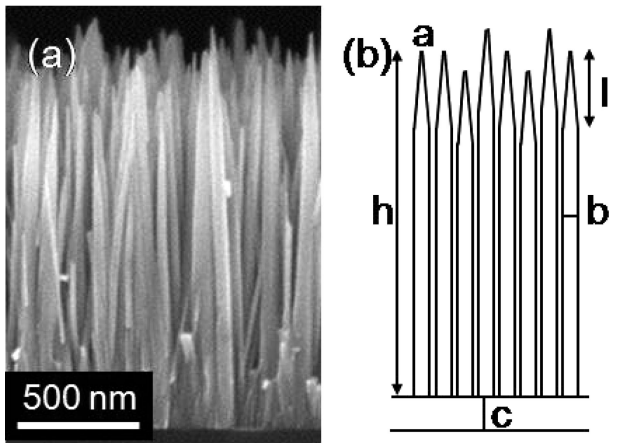

Figure 1. Example of a ZnO NRA. (a) Cross section SEM image of a highly tapered ZnO NRA (190 mM DAP, 60 °C growth temperature, 18 h growth time). (b) Schematic representation of the corresponding nanorod parameters extracted via software analysis.

ARC structure was characterized by field emission SEM (Zeiss) and X-ray diffraction (XRD, Rigaku). Analyzing cross sectional SEM images of each ZnO NRA (e.g., Figure 1a) using ImageJ, we obtained an average value over at least five measurements for various parameters including nanorod tip diameter a, diameter of the nontapered region b, thickness of the fused base layer c, overall nanorod length h, and length of the tapered region l, as schematically represented in Figure 1b. From the top view SEM images, we also determined via software analysis the area fraction of ZnO (~0.7 for all NRAs) and used it as the NRA volume fraction f of the nontapered region, because nanorods synthesized using the two-step seeding and growth procedure are vertically oriented.[19,20] Absolute hemispherical reflectance measurements were carried out with a UV−vis-near IR spectrophotometer (Cary) and an integrating sphere (Labsphere) with a sampling spot of 3 mm × 13 mm at normal incidence. Weighted reflectance R_w was calculated by normalizing the reflectance spectra with the internal quantum efficiency spectra of a typical multicrystalline Si solar cell and the terrestrial global solar spectrum (AM1.5).[9] Comparisons with a multicrystalline Si solar cell with a silicon nitride (SiN) SLARC were made.

Variations in the NRA growth conditions strongly influenced the morphology of the textured ZnO ARCs, as shown by the SEM images (Figure 2). For example, at a growth temperature of 92.5 °C, the tips of the ZnO nanorods changed from a flat top (Figure 2a) to a tapered shape (Figure 2c) with the addition of DAP in the growth solution. In the presence of DAP, an increase in growth time simultaneously increased nanorod length and decreased tip diameter, as seen for samples grown for 30 min (Figure 2b) and 45 min (Figure 2c). Decreasing the growth temperature to 60 °C significantly reduced the growth rate, while creating highly tapered nanorods with a tip diameter of ~10 nm (Figure 2d). XRD spectra of all ZnO NRAs revealed a strong (002) peak at $2\theta = 34.4°$ (Figure 2f) and no other crystallographic peaks, indicating that the nanorods are highly aligned, in agreement with SEM images. In contrast, the sol−gel ZnO film

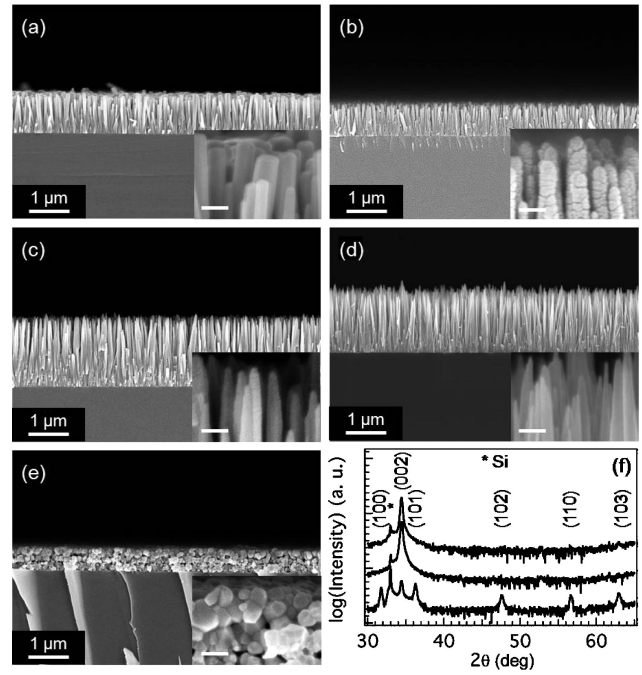

Figure 2. Cross section SEM images of nanostructured ZnO ARCs deposited under different conditions. (a) Flat top nanorods. (b) Tapered nanorods, 30 min growth time. (c) Tapered nanorods, 45 min growth time. (d) Highly tapered nanorods, 18 h growth time. (e) Sol−gel film. Inset, high magnification view of the samples (scale bar, 100 nm). (f) XRD spectra of flat top nanorods (top), highly tapered nanorods (middle), and sol−gel film (bottom), with ZnO peaks indexed.

contained unaligned pores (Figure 2e) and randomly oriented crystallites (Figure 2f).

Comparisons of the reflectance spectra of ZnO NRAs with each other and with other dielectric films reveal the importance of morphology on ARC performance. First, all NRAs exhibited significantly lower reflectance spectra (Figure 3) and R_w values (Table 1) compared with the sol−gel ZnO film with randomly oriented ~200 nm diameter pores. In other words, a combination of increased pore alignment and decreased pore diameter appears to improve antireflection response. Second, compared with a ZnO NRA with a flat top surface (Figure 3, red), a tapered NRA synthesized in the presence of DAP eliminated the optical interference fringes (Figure 3, orange). The elimination of interference is due to a rough ZnO−air interface from tapering of the nanorod tips (Figure 2c, inset) and variation in nanorod length, as will be shown later. More significantly, differences in NRA morphology caused by changing the synthesis conditions significantly altered the macroscale ARC response. For example, the tapered NRA grown at 92.5 °C exhibited a weak monotonic decrease in reflectance with wavelength (Figure 3, orange), resulting in a relatively high R_w of 13.6% (Table 1). The highly tapered NRA grown at 60 °C showed the same trend but with a stronger wavelength dependence and significantly lower reflectance for wavelengths greater than 500 nm (Figure 3, black), leading to a R_w of 6.6% (Table 1). In contrast, an optimized quarter wavelength SiN SLARC on a multicrystalline-Si solar cell exhibited a highly wavelength dependent reflectance response

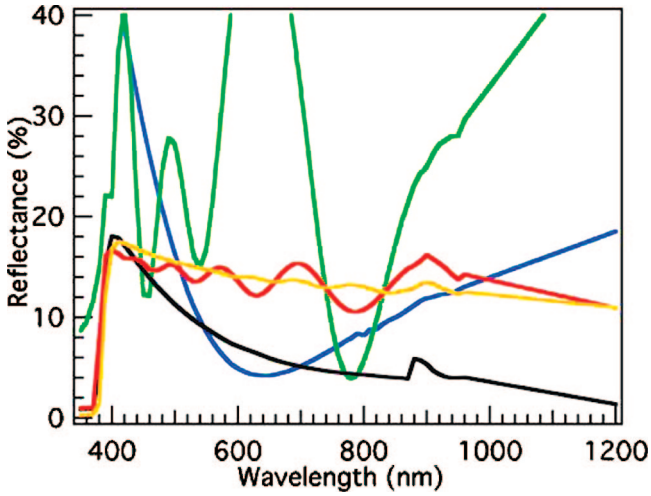

Figure 3. Front reflectance spectra of flat top NRA (red), tapered NRA (orange), sol−gel film (green), optimized SiN SLARC on Si PV cell with metallic contact (blue), and highly tapered NRA (black). The bump at 900 nm is due to a detector change during data collection.

Table 1. Measured Nanorod Parameters and R_w Values for ZnO NRA and Other ARCs[a]

sample	a (nm)	b (nm)	c (nm)	l (nm)	h (μm)	R_w (%)
flat top	51	51	40	NA	0.95	12.2
tapered	18	53	120	210	1.7	13.6
highly tapered	10	45	100	330	1.5	6.6
sol−gel	NA	NA	NA	NA	0.55	30.3
SLARC	NA	NA	NA	NA	0.08	7.8

[a] The nontapered region volume fraction f was found to be ~0.7 for all NRAs.

(Figure 3, blue) with a minimum at 640 nm due to destructive interference, and a R_w of 7.8% after subtracting the contribution from metallic contacts.[9] While the highly tapered NRA did not reach the same minimum visible reflectance compared with the SLARC, its significantly reduced wavelength dependence and the enhanced reflectance suppression between 700 and 1200 nm are primarily responsible for the improvement in R_w. In short, orientation of the air pores, roughening of the ZnO-air interface, and morphological changes such as nanorod tip tapering all contribute to the improvement in the performance of ZnO NRA ARCs.

Since different synthesis conditions simultaneously changed several parameters in the resulting NRA ARCs (Table 1), to isolate the contribution of each nanorod parameter (a, c, l, or f) to the performance of the ARCs, we employed RCWA to calculate the front hemispherical reflectance spectra from the extracted nanorod parameters (Table 1) by systematically varying the value of one parameter while holding the other parameters to their default extracted values (Table 1). RCWA is a rigorous methodology for structures periodic in one or two dimensions that computes the electromagnetic modes present in each layer, then applies boundary conditions between the layers to calculate reflected and transmitted orders.[24] Optical constants for ZnO from literature were used for the calculations.[25] For RCWA, we subdivided each NRA into 12 layers: a bottom fused layer with $f = 1$, a nontapered NRA layer with $f = 0.7$, and a 10 layer stack for the tapered region. To approximate the tapering of each NRA, we calculated diameter d and f for each layer in the stack using linear interpolation of the bottom of the tapered region ($d = b$, $f = 0.7$) and the top of the tapered region ($d = a$, $f = 0.7a^2/b^2$). To approximate the SEM observations, we also determined the effect for a linear variation in h of 10% by calculating the reflectance spectra for NRAs each with uniform length ranging from $h - 10\%$ to $h + 10\%$ at 0.5% increment, and then averaging the resulting 21 spectra. Distributions in a and b were not accounted for because they were folded into the average volume fraction for each layer in RCWA. Front hemispherical reflectance spectra for the RCWA simulations were performed using Grating Diffraction Calculator, a commercial package that runs in Matlab. By varying one parameter at a time, the RCWA calculated front hemispherical reflectance spectra and subsequently the corresponding R_w enabled us to isolate the effect of each morphological factor.

We found that good agreement between calculated and experimental reflectance spectra can be achieved through the elimination of interference fringes via a combination of nanorod tip tapering ($a < b$) and variation in nanorod length h. The reflectance spectra of a flat top NRA with uniform length exhibited very strong interference fringes of ~20% intensity (Figure 4a, red). The introduction of length variation dramatically decreased the interference fringe intensity to ~5% (Figure 4a, blue), similar to the experimental data (Figure 4a, black). In addition, for the flat top NRA, the R_w value from experiment of 12.2% (Table 1) is very close to the value from RCWA of 12.5% (Table 2). Further increase in length variation to 20% did not significantly change the strength of the interference fringes (Supporting Information). Thus, there is very good agreement between measured response and RCWA results for the flat top NRA.

According to RCWA, tapering of the nanorod tips also contributes to suppression of interference fringes in the reflectance spectra. For example, a highly tapered NRA (a = 10 nm, Table 1) with uniform length exhibited interference fringes with an intensity of ~4% (Figure 4b, red), much lower than the flat top rods (Figure 4a, red). The addition of a 10% length variation to this system reduced the interference fringe intensity to <1% (Figure 4b, blue), similar to the experimental data which showed no interference fringes (Figure 4b, black). While both experimental and calculated spectra for the highly tapered NRA showed qualitative agreement in that both spectra monotonically decreased as wavelength increased (Figure 4b), they exhibited significantly different R_w values of 6.6% (Table 1) and 9.0% (Table 2), respectively. This indicates that the tapering of the ZnO nanorods results in a more complex shape than our model of a linear decrease in diameter, preventing us from a quantitative comparison between experiment and theory. Nevertheless, we believe our model captures enough details of the experimental system to predict the effect of changing one parameter at a time, as shown below.

We found the shape of the reflectance spectra to be strongly influenced by c, the thickness of the fused ZnO bottom layer (Figure 4c). By changing c from 75 to 100 nm while keeping the other parameters constant for a highly

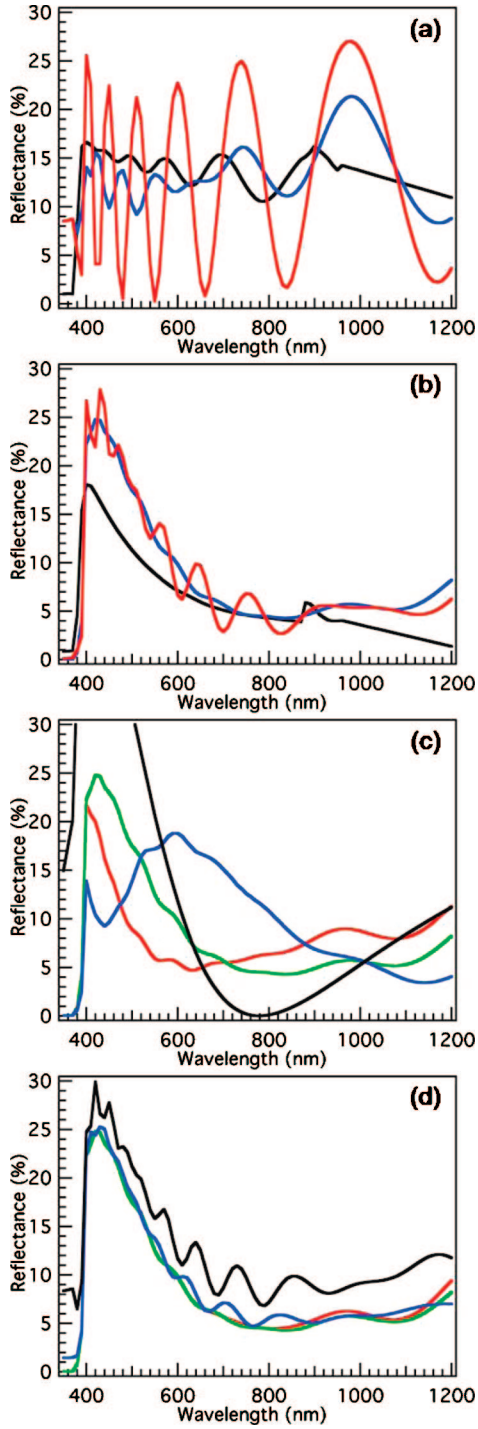

Figure 4. Effect of ZnO nanorod morphology on reflectance spectra of NRA ARCs calculated via RCWA. (a) Flat top NRA with uniform length (red), 10% length variation (blue), and experimental data (black). (b) Highly tapered NRA with uniform length (red), 10% length variation (blue), and experimental data (black). (c) Highly tapered NRA with bottom layer thickness c of 75 nm (red), 100 nm (green), 150 nm (blue), and 100 nm ZnO SLARC (black). (d) Highly tapered NRA with tip diameter a of 2 nm (red), 10 nm (green), 30 nm (blue), and 45 nm (black).

tapered NRA, the wavelength of reflectance minimum λ_{min} shifted from 600 nm (Figure 4c, red) to 800 nm (Figure 4c, green). A further increase in c to 150 nm shifted λ_{min} out of the experimental wavelength range and introduced a maximum in reflectance at 600 nm (Figure 4c, blue). This behavior is similar to that of a SLARC ($\lambda_{min} = 4nc$) for $n = 2$, which matches the refractive index of dense ZnO at 633 nm; however, as we noted before, the reflectance spectra of NRA ARCs are less wavelength dependent than that of a SLARC, such as a 100 nm thick ZnO film (Figure 4c, black). R_w derived from RCWA spectra for c between 75 and 150 nm increased from 7.5% to 12.7% (Table 2), suggesting that tailoring the fused layer thickness may be important in optimizing ARC performance. In short, both experimental data and RCWA calculations indicate that a tapered ZnO NRA with a fused bottom layer behaves like a modified SLARC with greater broadband suppression of reflection, particularly for the longer wavelengths.

Table 2. Effect of Variation of One Nanorod Parameter on R_w Values Derived from RCWA Spectra for Highly Tapered ZnO NRA ARC ($f = 0.7$) with Parameters that Are Varied, and the Resulting R_w Are in Bold

a (nm)	b (nm)	c (nm)	l (nm)	h (μm)	R_w (%)
2	45	100	330	1.5	**9.2**
4	45	100	330	1.5	**9.1**
10	45	100	330	1.5	**9.0**
20	45	100	330	1.5	**9.0**
30	45	100	330	1.5	**9.5**
45	45	100	330	1.5	**12.5**
10	45	**75**	330	1.5	**7.5**
10	45	**90**	330	1.5	**8.1**
10	45	**100**	330	1.5	**9.0**
10	45	**125**	330	1.5	**11.3**
10	45	**150**	330	1.5	**12.7**

A noticeable improvement of the ARC performance can be achieved with a moderate degree of nanorod tip tapering, according to RCWA calculations. When a was decreased from 45 nm, that is, flat top nanorods (Figure 4d, black), to 30 nm (Figure 4d, blue), the reflectance spectra shifted downward across the entire wavelength range, and the interference fringes also decreased in intensity. Further reductions in the tip diameter to 10 nm (Figure 4d, green) and 2 nm (Figure 4d, red) eliminated the interference fringes while maintaining the overall shape of the reflectance spectra. From the corresponding R_w, we found that decreasing a to 30 nm improved R_w from 12.5% to 9.5%, and further reductions in tip diameter only resulted in a 0.5% improvement in R_w (Table 2). We also examined the effect of f and l on NRA ARC performance, and found that they affected the reflectance spectra in minor ways (Supporting Information). In summary, through a systematic examination of the effect of nanorod morphology on the reflectance spectra of ZnO NRAs on Si, we demonstrated that variation in nanorod length, thickness of the fused bottom layer, and tapering of nanorod tips all contribute to the improvement of ZnO NRA ARC performance by introducing broadband suppression of reflectance and eliminating interference fringes. These findings are in agreement with prior explorations of the idealized refractive index gradient of structured antireflection coatings.[26] The tapered nature of the ZnO NRAs leads to an impedance matching of the silicon to the air through a gradual reduction of the effective index away from the surface, and behave similarly to lithographically patterned subwavelength textured dielectric ARCs operating in the mid-infrared when the rod diameter is scaled to the wavelength.[27]

By using aqueous solution synthesis of tapered ZnO NRAs, we demonstrated a simple, large area fabrication of sub-wavelength textured ARCs for visible-near IR wavelengths, which would otherwise require complicated techniques such as e-beam or nanoimprint lithography followed by etching. Through modifications of NRA synthesis, in particular to tailor the bottom layer thickness and to further control nanorod shape, we may be able to further optimize the refractive index gradient and thus decrease reflectance.[26]

We fabricated textured ZnO ARCs via low temperature aqueous solution deposition of highly aligned ZnO NRAs. By controlling the solution growth conditions, we tuned the morphology of the ZnO NRAs and showed that presence of a bottom fused layer combined with tapering of nanorod tips resulted in broadband suppression of reflectance, with R_w of 6.6% for a 1.5 μm highly tapered ZnO NRA. RCWA calculations of the effect of various nanorod parameters on ARC performance suggested that the highly tapered ZnO NRA ARC behaved like a modified SLARC with reduced wavelength dependence due to the nanoscale morphology, because the tapering produces impedance matching between Si and air through a gradual reduction of the effective refractive index away from the surface. Variation in nanorod length, presence of a fused ZnO base layer, and introduction of tip tapering all contributed to the decrease in reflectance and the elimination of interference fringes, in good qualitative agreement with experimental results. Because of the low temperature and substrate independent processing, these novel textured ZnO ARCs may be suitable for low cost, large area, PV devices and other antireflection applications.

Acknowledgment. We thank D. Olson and E. Spoerke for helpful discussions and J. Finn for reflectance measurements. This project is financially supported by the LDRD program at Sandia National Laboratories. Sandia is a multiprogram laboratory operated by Sandia Corporation, a Lockheed Martin Company, for the United States Department of Energy under Contract No. DE-AC04-94AL85000.

Supporting Information Available: Details on the ZnO NRA synthesis, further discussion on the effect of synthesis conditions on nanorod shape and ARC performance, and RCWA results from varying additional parameters. This material is available free of charge via the Internet at http://pubs.acs.org.

References

(1) Green, M. A. *Silicon Solar Cells: Advanced Principles and Practice*;Bridge: Sydney, 1995.
(2) Lalanne, P.; Morris, G. M. *Nanotechnology* **1997**, *8*, 53.
(3) Kanamori, Y.; Hane, K.; Sai, H.; Yugami, H. *Appl. Phys. Lett.* **2001**, *78*, 142.
(4) Koynov, S.; Brandt, M. S.; Stutzmann, M. *Appl. Phys. Lett.* **2006**, *88*, 203107.
(5) Sun, C. H.; Jiang, B.; Jiang, P. *Appl. Phys. Lett.* **2008**, *92*, 061112.
(6) Striemer, C. C.; Fauchet, P. M. *Appl. Phys. Lett.* **2002**, *81*, 2980.
(7) Zaidi, S. H.; Ruby, D. S.; Gee, J. M. *IEEE Trans. Electron Devices* **2001**, *48*, 1200.
(8) Ruby, D. S.; Zaidi, S. H.; Narayanan, S.; Damiani, B. M.; Rohatgi, A. *Solar Energy Materials and Solar Cells* **2002**, *74*, 133.
(9) Ruby, D. S.; Wilbanks, W. L.; Fleddermann, C. B. In Conference Record of the First WCPEC, IEEE: Piscataway, NJ, 1994; p. 1335.
(10) Orgassa, K.; Rau, U.; Nguyen, Q.; Schrock, H. W.; Werner, J. H. *Prog. Photovolt.* **2002**, *10*, 457.
(11) Ramanathan, K.; Contreras, M. A.; Perkins, C. L.; Asher, S.; Hasoon, F. S.; Keane, J.; Young, D.; Romero, M.; Metzger, W.; Noufi, R.; Ward, J.; Duda, A. *Prog. Photovolt.* **2003**, *11*, 225.
(12) Takato, H.; Yamanaka, M.; Hayashi, Y.; Shimokawa, R.; Hide, I.; Gohda, S.; Nagamine, F.; Tsuboi, H. *Jpn. J. Appl Phys.* **1992**, *31*, L1665.
(13) Doshi, P.; Jellison, G. E.; Rohatgi, A. *Appl. Opt.* **1997**, *36*, 7826.
(14) Aberle, A. G. *Sol. Ene. Mat. Sol. Cel.* **2001**, *65*, 239.
(15) Richards, B. S. *Prog. Photovolt.* **2004**, *12*, 253.
(16) Kennedy, S. R.; Brett, M. J. *Appl. Opt.* **2003**, *42*, 4573.
(17) Richards, B. S.; Rowlands, S. F.; Honsberg, C. B.; Cotter, J. E. *Prog. Photovolt.* **2003**, *11*, 27.
(18) Xi, J.-Q.; Schubert, M. F.; Kim, J. K.; Schubert, E. F.; Chen, M.; Lin, S.-Y.; Liu, W.; Smart, J. A. *Nat. Photon.* **2007**, *1*, 176.
(19) Greene, L. E.; Law, M.; Tan, D. H.; Montano, M.; Goldberger, J.; Somorjai, G.; Yang, P. *Nano. Lett.* **2005**, *5*, 1231.
(20) Lee, Y.-J.; Sounart, T. L.; Scrymgeour, D. A.; Voigt, J. A.; Hsu, J. W. P. *J. Cryst. Growth* **2007**, *304*, 80.
(21) Sounart, T. L.; Liu, J.; Voigt, J. A.; Hsu, J. W. P.; Spoerke, E. D.; Tian, Z. R.; Jiang, Y. *Adv. Funct. Mater.* **2006**, *16*, 335.
(22) Lee, Y.-J.; Sounart, T. L.; Liu, J.; Spoerke, E. D.; McKenzie, B. B.; Hsu, J. W. P.; Voigt, J. A. *Cryst. Growth Des.* in review.
(23) Ohyama, M.; Kozuka, H.; Yoko, T. *Thin Solid Films* **1997**, *306*, 78.
(24) Moharam, M. G.; Gaylord, T. K. *J. Opt. Soc. Am. A.* **1986**, *3*, 11.
(25) Yoshikawa, H.; Adachi, S. *Jpn. J. Appl. Phys.* **1997**, *36*, 6237.
(26) Southwell, W. H. *J. Opt. Soc. Am. A* **1991**, *8*, 549.
(27) Hobbs, D. S.; MacLeod, B. D. *Proc. SPIE* **2005**, *5786*, 349.

NL080659J